Synthesis, Characterization, DNA binding and Photocleavage studies of transition metal (II) pyrene Schiff base complexes

Mohanambal D.[1,2*] and Arul Antony S.[3]
1. Research and Development Centre, Bharathiar University, Coimbatore, Tamilnadu, INDIA
2. Department of Chemistry, Loyola Institute of Technology, Palanchur, Chennai-600 123, INDIA
3. PG and Research Department of Chemistry, Presidency College (Autonomous), Chennai–600 005, INDIA
*mohanachem2010@gmail.com

Abstract
The metal complexes containing Co (II), Mn (II), Ni (II), Cu (II) and Zn (II) with corresponding ligands have been prepared. Pyrene -1- aldehyde, 4-aminoantipyrine Schiff base ligands are synthesized and their characterization is also carried out. The spectroscopic techniques like FTIR, UV-Vis, ^{1}H and ^{13}C NMR and magnetic measurements suggested, the square planner structure for the complex. The cleavage mechanism of supercoil plasmid DNA induced by Cu (II) complexes is also studied.

Keywords: DNA Binding, Schiff base, metal complexes, Agarose gel electrophoresis.

Introduction
Over the past few decades, Schiff bases ligands are used in broad area of research such as medicinal chemistry, pharmaceutical and bio medicinal applications and their transition metal complexes are applied in biological activities such as antitumor, antipyretic, antimicrobial, antiviral, anti- inflammatory and antifungal activity[7]. An amino pyrazole compound was used for the modified synthesis of pyrazolotriazine heterocyclic compound which is a starting point of diazotization and diazocoupling with active methylene group[3]. Phenazone and its derivatives are conventional organic compounds used mainly as acting to relieve pain and antipyretic drugs[8,17].

One of the familiar organic moieties such as antipyrine derivatives is 4-aminoantipyrine which is used for the collateral against oxidative stress as well as prophylactic of some diseases including cancer and these are important directions in medicine and biochemistry[9]. Responsive oxygen species including free radicals prompted a lessening in the cancer prevention agent limit and may create other receptive species that harm the living cell. Oxidative pressure may emerge in a natural framework after an expanded introduction to oxidants, so that the cancer prevention agents assume a noteworthy job in securing organic frameworks against such dangers[12].

Transition metal complexes of pyrazole derivatives have received additional attention as useful metastatic tumour agents. Formation of coordination bond brings intensive changes in biological properties of matter and co-jointly in metal ions. Biological importance of various structural teams of many pyrazole ring systems is related to the well-known Cu (II) particle from a series of coordination compounds with well-defined structures recently. It plays a very important role within the various biological processes that involve lepton transfer reactions or the activation of some anti-tumour substances[6].

The role of those enzymes is the results of two processes such as the reduction of the Cu^{2+} ion to Cu^{+} and the fixation of the molecular atomic number eight. The Cu^{2+} particle is concerned within the expression of genes for the metal-binding proteins[15] and it is also found in copper-protein combinations displaying a pseudo tetrahedral symmetry and having effects in bio-systems. Through aminoxidase, copper interferes in the metabolism of the conjunctive tissue contributing to the torpidity of vascular sides[2]. Taking into account the daily necessary quantity of Cu (II) in the organism (2-3 mg/day), its distribution and metabolism in the organism, toxicity and numerous simple or complex combinations of copper are used in the treatment of a variety of diseases including inflammatory processes, cancer, ulcers, nervous system and heart diseases etc.

As a genetic instructor, DNA is the pharmacological target due to the availability of the genome sequence in advanced clinical trials[11], which play key physiological roles in the life process. An interaction between small molecules and DNA via covalent or non-covalent interactions is leading to alteration or inhibition of DNA function[18]. However, mechanism of interactions between drug molecules and DNA is still little known as compared to the protein-based drug targets. Therefore, it is considerable to characterize the binding mechanism of drugs to DNA with more simple experimental methods and the molecular docking methods[16]. This has brought the possibility of understanding the structural features of DNA and improved drug entities with clinical efficacy.

Material and Methods
Synthesis of 1,5-dimethyl-2-phenyl-4-((pyren-1-ylmethylene)amino)-1H-pyrazol- 3(2H)-one(1): 10 ml ethanolic solution of 1-Pyrenecarboxaldehyde (232mg, 1.01mmol) was added to 10ml of ethanolic solution of 4-aminoantipyrine (212.6mg, 1.05mmol) with constant stirring and then two drops of glacial acetic acid were added. Then the reaction mixture was refluxed for 12hrs. The resulting precipitate was filtered. The filtered solid was washed with acetone and purified by crystallization from

acetonitrile. Bright golden yellow crystals were obtained PAPY (Scheme 1).

Synthesis of Pyrene-1,4-aminoantipyrine Schiff base Metal (II) complexes: 20 ml of methanol solution of MCl_25H_2O (0.26g / 1mM) [M (II) = Cu (II), Ni (II), Co (II) Zn (II) and Mn (II)] was slowly added to the 15ml methanolic solution of pyrene-1,4-aminoantipyrine Schiff base ligand (0.835g / 2mM) with constant stirring under nitrogen atmosphere with the addition of triethyl amine (0.05ml, 0.36mmol) until a ferment colour appeared. Then 10ml of aq KOH (0.5g, 0.89mmol) was added and the mixture was refluxed for 12hrs and allowed to cool. Solid complex thus obtained was separated, washed with acetone and dried in vacuum over CaO (Scheme 2).

Results and Discussion

Novel Pyrene Schiff base ligands and their metal complexes were synthesized by the reaction of ligands with the appropriate mole ratios of M (II) halide in ethanol. They are air stable for extended periods and soluble in MeOH, CH_2Cl_2, DMSO and DMF. The molar conductivities of the Co (II) and Mn (II) complexes were found to be around 94 $Ohm^{-1}cm^{-1}M^{-1}$ in CH_2Cl_2 and for Cu (II) and Zn (II)complex as ~95$Ohm^{-1}cm^{-1}M^{-1}$ suggesting that Co (II)/ Mn (II) complexes are 2:1 electrolytes whereas Cu (II) and Zn (II) complex is 1:1 electrolyte. The elemental analyses and molar conductance measurement confirmed their composition as $[ML_2]\ Cl_2$ for Co (II)/Mn (II) and $[ML_2]$ for Cu (II) and Zn (II) complexes. Analytical data of the ligands and complexes are listed in table 1.

^{1}H NMR Spectra of Pyrene-1,4-aminoantipyrine Schiff base ligand (PAPY): The ^{1}H NMR spectra of PAPY ligand were recorded in $CDCl_3$ solution using TMS as internal standard (Fig.1), exhibited signals around 10.96 ppm due to the azomethine (-CH=N) protons. Pyrene unit appears at 8.07 to 8.91ppm get multiple signals. The aromatic and anti-pyrane ring protons resonate as complex multiplet in the region 7.37-7.98 ppm. The signal due to methyl group attached to the anti-pyrine ring C-CH_3 and N-CH_3 is observed almost at their respective positions 2.57 and 3.12ppm respectively. The ^{1}H NMR signals of ligands and their assignments are presented in table 2.

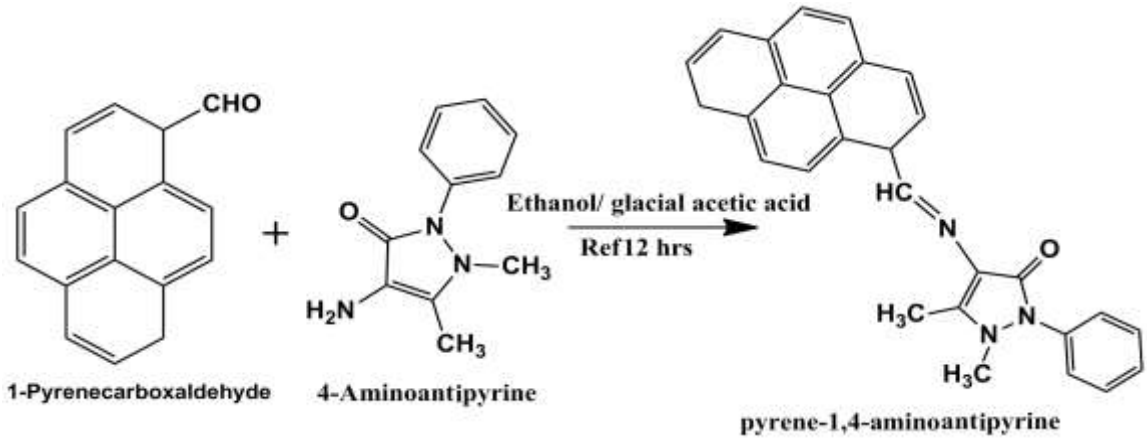

Scheme 1: Synthesis of pyrene-1, 4-aminoantipyrine Schiff base ligand (PAPY)

Table 1
Composition and physical characteristics of pyrene-1, 4-aminoantipyrine Schiff ligand and their complexes

Compounds	Molecular Formula	Color	Found (Calculated) %				M.P (°C)	M.Wt	Ω ($Ohm^{-1}\ cm^{-1}\ M^{-1}$)
			C	H	N	O			
PAPY	$C_{28}H_{23}N_3O$	Green Yellow	80.55 (79.98)	5.67 (4.56)	10.08 (9.93)	03.85 (03.12)	284	417.50	--
$(PAPY)_2Cu$	$C_{56}H_{46}N_6O_2Cu$	Brown	74.86 (76.11)	5.23 (4.01)	9.54 (9.26)	3.82 (3.67)	>300	898.55	95
$(PAPY)_2Mn$	$C_{56}H_{46}N_6O_2Mn$	Pale Yellow	75.11 (79.87)	5.24 (4.15)	9.23 (9.02)	3.47 (3.33)	>300	889.31	145
$(PAPY)_2Co$	$C_{56}H_{46}N_6O_2Co$	Dark Brown	56.87 (56.67)	3.97 (3.89)	9.56 (9.34)	10.89 (10.76)	>300	893.30	145
$(PAPY)_2Ni$	$C_{56}H_{46}N_6O_2Ni$	Brown	52.87 (52.13)	3.76 (3.34)	8.98 (8.77)	10.23 (10.02)	>300	892.30	91
$(PAPY)_2Zn$	$C_{56}H_{46}N_6O_2Zn$	Colorless	55.67 (55.11)	3.78 (3.43)	9.65 (9.22)	10.78 (10.53)	>300	898.30	95

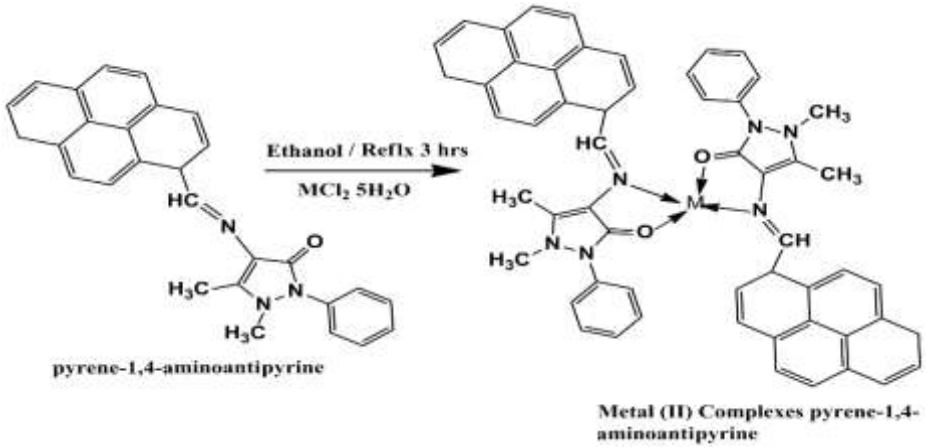

Scheme 2: Synthesis of pyrene-1, 4-aminoantipyrine Schiff base Metal (II) complexes

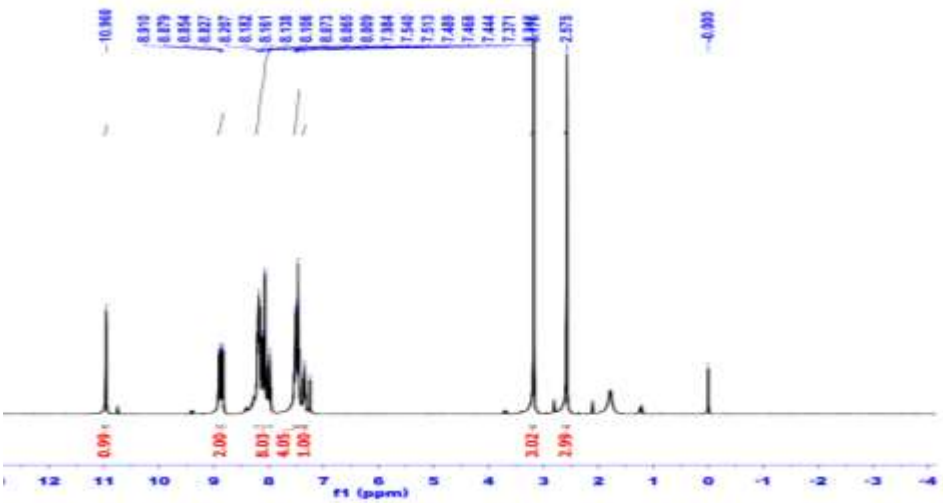

Fig. 1: ^{1}H NMR spectrum of pyrene-1,4-aminoantipyrine Schiff base ligand (PAPY)

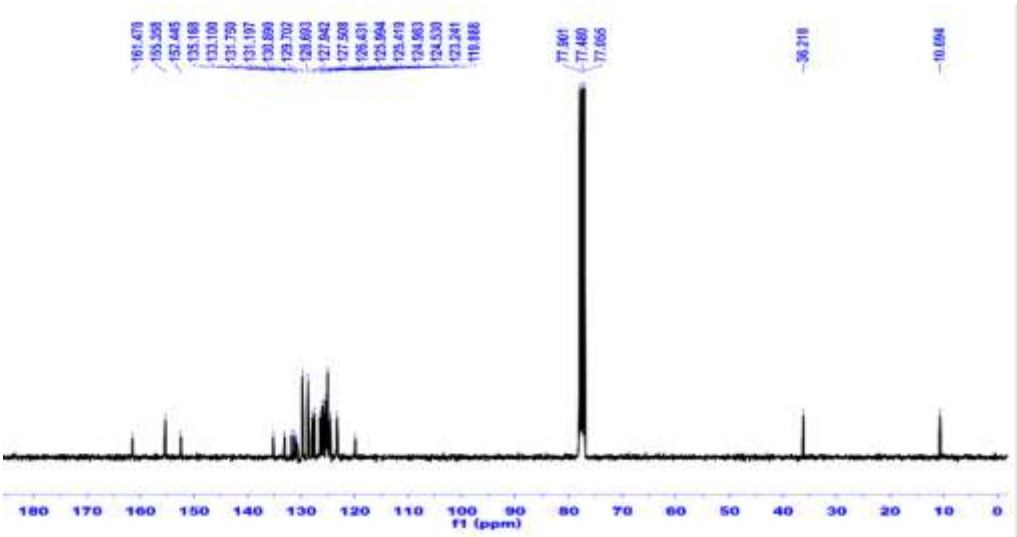

Fig. 2: ^{13}C NMR spectrum of pyrene-1,4-aminoantipyrine Schiff base ligand

^{13}C NMR Spectra of pyrene-1,4-aminoantipyrine Schiff base ligand (PAPY): ^{13}C NMR spectra (Fig. 2) of the ligands show a signal at δ 161.47ppm for C=O group of anti-pyrine which would be bonded to the metal. The signals appear at δ 36.21ppm (for methyl carbon of CH_3-N) and at δ 10.69ppm (for methyl carbon of CH_3-C-3), a multiplet for aromatic carbon between δ 119.88-129.70 ppm for C-4 and C-3 carbons of antipyrine respectively. The signals observed between δ at 130.89 – 135.16 ppm were assigned as pyrene group of ring while the azomethine carbon was observed at δ 161.4 ppm.

FTIR Spectra of PAPY ligand and Complexes: Selected infrared absorption frequencies of both the ligands and their complexes are given in table 3. The comparison of the spectra of the ligands and their complexes supports the neutral tridentate O, O, N- chelating nature of the ligands. The spectra of all compounds (Fig. 5 and 6) exhibit two medium intensity bands around 307cm^{-1} and 2923 cm^{-1} corresponding to asymmetric and symmetric stretching vibrations of the aromatic C-H groups[13].

The aliphatic CH_3 groups lead to two small bands around 2883cm^{-1} due to the stretching modes while their deformation vibration gives strong bands at 1143cm^{-1}. The absorption band at 1542cm^{-1} due to the azomethine bond of the free ligand molecule hypsochromic shifted to 30cm^{-1} upon coordination to the metal ion. This indicates that the nitrogen atom of the C=N bond is involved in the coordination. All compounds display an intense band in the range of 1643-1749cm^{-1} and 1590-1685cm^{-1} corresponding to $\upsilon_{C=O}$ of antipyrine ring respectively.

The $\upsilon_{C=O}$ band for all the complexes appears at lower frequencies compared to that for the free ligand, which is due to the participation of carbonyl oxygen atom of antipyrine ring. The zinc complex shows a strong band at 777cm^{-1} assigned as Zn-Cl stretching vibrations.Appearance of new bands in the spectra of all the complexes in the regions 490-540cm^{-1} and 450-540cm^{-1} would attribute to υ_{M-O} and υ_{M-N} respectively. The IR spectra of the chloro complexes (Zn) reveal an additional new band at 761cm^{-1} which can be assigned to υ_{M-Cl}. The presence of chlorine atom in complex is proved by elemental chemical analysis and its inner-sphere position is confirmed by the absence of qualitative reaction with $AgNO_3$ solution. These shifts and the new bands demonstrate that the oxygen of carbonyl and nitrogen atom of azomethine has formed a coordinative bond with the transition metal ions.

Table 2
^{1}H NMR and ^{13}C NMR Spectra data for PAPY (PAPY)

Compound	^{1}H (δ, ppm)	Assignment	^{13}C (δ, ppm)	Assignment
PAPY	7.39 – 7.49	Bezene in antipyrine proton ≈ 5H	118.1-129.6	Aromatic anti-pyrene
	9.81	C-H (γ-pyrone) ≈ 1H	130.89-135.16	Carbon (pyrene)
	10.96	C-H (azomethine) ≈ 1H	161.4	azomethine
	3.55	N-methyl ≈ 3H	156.1	C=O
	2.57	Methyl ≈ 3H	152.5	ethylene
	3.52	Methine in pyrene unit	35.8	N-methyl
	8.02 -8.91	Pyrene unit proton ≈9H	10.1	methyl

Table 3
Key FTIR bands (cm^{-1}) of PAPY ligand and their complexes

Compound	υ_{C-H}	$\upsilon_{C=N}$	$\upsilon_{C=O}$	υ_{N-N}	$\upsilon_{C=O}$	υ_{M-N}	υ_{M-O}	υ_{M-Cl}
PAPY	2929	1542	1716	1039	1662	---	---	----
$(PAPY)_2Cu$	2923	1583	1749	1029	1685	443	534	761
$(PAPY)_2Mn$	2906	1585	1655	1016	1618	457	514	761
$(PAPY)_2Ni$	2923	1606	1737	1019	1643	453	545	----
$(PAPY)_2Zn$	2923	1542	1685	1016	1598	433	545	----

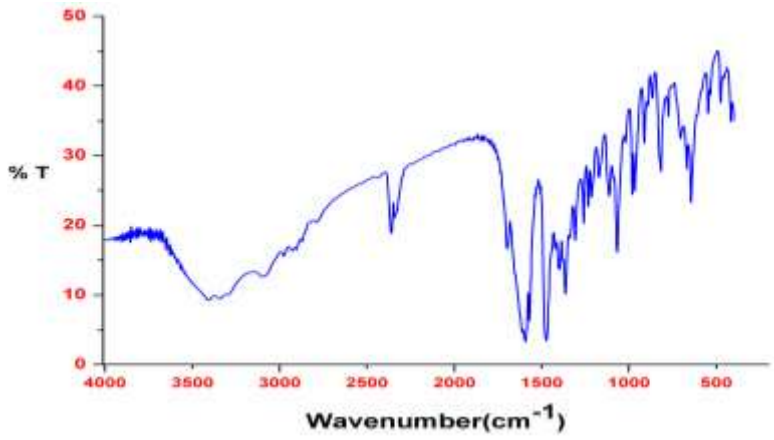

Fig. 5: FTIR spectrum of PAPY ligand

Electronic spectra of PAPY ligand and its complexes: The electronic spectra of the ligand and their complexes with tentative assignments are presented in fig. 7 to fig. 9. The optical spectrum of the ligands shows two band maxima at 35,971 and 45,871cm^{-1} corresponding to n-π* and π-π* transitions[4] respectively. In complexes, both n-π* and π-π* bands are found as blue shifted and appeared in the region 35,303-45,662cm^{-1} and 37,313-50,505cm^{-1} regions respectively compared to that of free ligand.

Manganese complexes are diamagnetic as expected for high spin Mn (II) (high spin, d^5, S=1/2) as in fig. 8. Four strong absorptions are observed in the ranges 21,613, 37,419, 43,993 and 49,918cm^{-1}. In this case, the low energy absorptions are likely to be due to the ligand-metal charge transfer transitions. The bands at 21,613cm^{-1} and 37,419 cm^{-1} can be assigned to d-d transition $^6A_1g \rightarrow {}^4T_1g$ and MLCT respectively.

The magnetic moment of [Mn $(PAPY)_2$] (5.8BM) shows the presence of five unpaired electrons and UV-Vis spectrum shows one d-d band at 21,897cm^{-1} assigned to the $^6A_1g \rightarrow {}^4T_1g$, ^4T_2g transition respectively for six coordinate high spin Mn (II) center possessing distorted octahedral geometry. Other band observed at 37,987cm^{-1} may be assigned to a charge transfer transition.

The complex Cu (II) may have a square planar coordination of the central metal ion by the surrounding ligands. Cu^{2+}ion having a d^9 configuration favour the formation of complexes with square planar geometry. The electronic spectrum of Cu^{2+} complex (Fig. 9) shows two spin allowed d-d bands around 14,625 and 29,330cm^{-1} region along with two charge transfer bands.

The spin allowed transitions were assigned as a combination of both $^1A_1g \rightarrow {}^1A_2g$ and $^1A_1g \rightarrow {}^1Eg$ transitions by assuming the difference in the energies of both b_2g (xy) and eg (xz, yz) levels is very little. The other spin allowed bands for these Cu^{2+} complexes assigned to the $^1A_1g \rightarrow {}^1B_1g$ transitions.

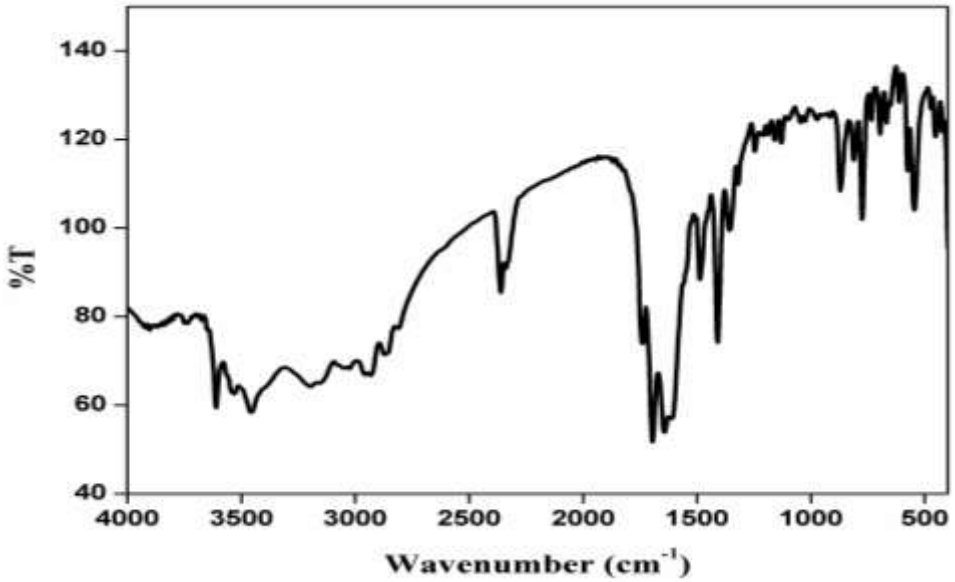

Fig. 6: FTIR spectrum of [Cu $(PAPY)_2$] Cl_2 Complex

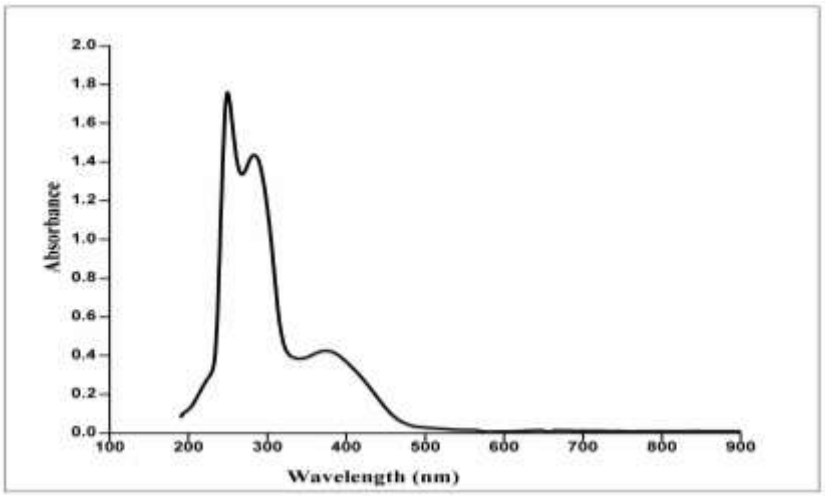

Fig. 7: Electronic spectrum of PAPY ligand

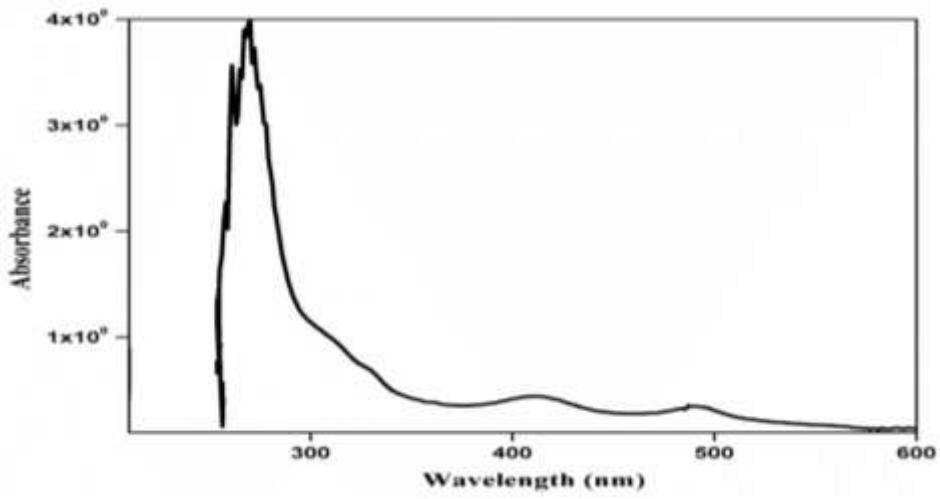

Fig. 8: Electronic spectrum of [Mn (PAPY)$_2$] Cl$_2$ Complex

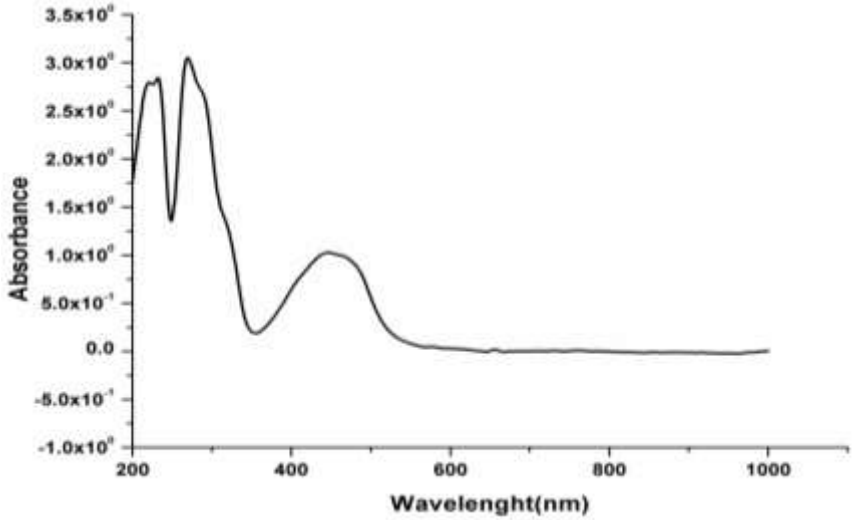

Fig. 9: Electronic spectrum of [Cu (PAPY)$_2$]Cl$_2$ Complex

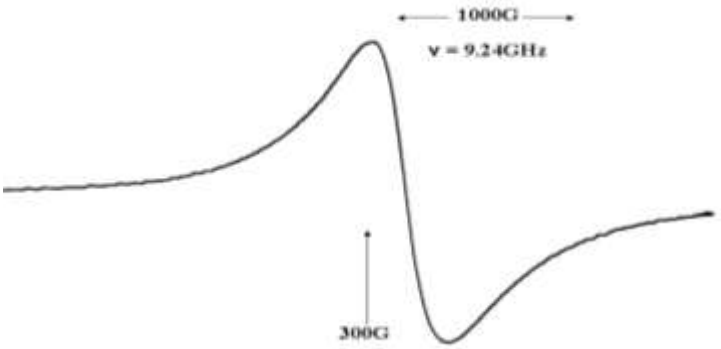

Fig. 10: ESR spectrum of [Mn (PAPY)$_2$]Cl$_2$ complex at 300 K

ESR Spectra of [Mn (PAPY)$_2$] Complex: The ground state of high spin octahedral Mn (II) complex is ^6A_1g and since there are no excited terms of sextet spin multiplicity, d-d transitions are doubly forbidden. However, some forbidden transitions occur and consequently, these transitions have an extremely low molar extinction coefficient value. The ESR spectrum of Mn (II) complex at room temperature shows the signals with g value $g_\parallel$= 2.11 and $g_\perp$ = 2.02. The $g_\parallel$ and $g_\perp$values are closer to 2 and $g_\parallel > g_\perp$ suggesting distorted octahedral geometry around Mn (II) ion. In addition, exchange coupling interaction was found to be as G = 1.09 from the expression $G = (g_\parallel-2) / (g_\perp-2)$.

The low temperature ESR spectrum of [Mn (PAPY)$_2$] is typical of Mn (II) complexes with a well-resolved six line hyperfine structure (~ 100 atom % ^{55}Mn, I = 5/2) (Fig.10). The measured parameters are $g_{II} \approx 1.98$, $g_\perp \approx 1.95$, $A_{II} \approx 170\times10^{-4}$ cm^{-1} and $A_\perp \approx 70 \times10^{-4}$ cm^{-1}. The corresponding

isotropic parameter is ‹g› 1.939 and ‹A› 107×10^{-4} cm^{-1}. The observed order in the spin Hamiltonian parameters (g_{II}> $g_{\perp}$ and A_{II}> $A_{\perp}$) suggests the distorted octahedral geometry around Mn (II) complex (Fig.11).

Electrochemical studies Mn (II) and Cu (II) Complexes: The electrochemical behaviors of mononuclear manganese (II) Schiff base complexes were investigated by cyclic voltammetry. Glossy carbon was used as the working electrode and potentials are reported versus Ag/AgCl reference electrode. The manganese (II) Schiff base mono metallic complexes exhibited relatively solubility in CH_2Cl_2 and CH_3CN solvents and their electrochemical properties were investigated in DMSO only.

The electrochemical behavior of the $[(PAPY)_2Cu]^{2+}$ complex (Fig. 12) has also been carried out in the range +1.5 to -1.5V and the cyclic voltammogram shows Cu(I)/Cu(II) oxidation process between +1.5V and 0V. Examination of the experimental data highlights the reduction of copper (II) as reversible. ΔEp = Epa – Epc is greater than 59 (145) and increases with increasing V. Ipa/Ipc is nearer to unity (0.65) and indicates the chemical reversibility of the redox changes.

All of them resemble of a reversible one electron transfer process. A cyclic voltammogram of Mn (II) complex (Fig.13) displays a reduction peak at Epc = 0.982V with a corresponding oxidation peak at Epa = 0.595V. The separation of this couple (ΔEp) is 0.387V at 100 mVs^{-1} and increases with scan rate. The difference between forward and backward peak potentials provides a rough evaluation of the degree of reversibility of electron transfer. Cyclic voltametric responses with scan rate 100 mVs^{-1} give evidence for a quasi- reversible one electron oxidation. The ratio of cathodic to anodic peak height (Ipa/Ipc) was less than one (0.56).

However, the peak current increases with increase of the square root of the scan rate establishing the electrode process as diffusion controlled. The separation in peak potentials increases at higher scan rates consistent with quasi reversible.

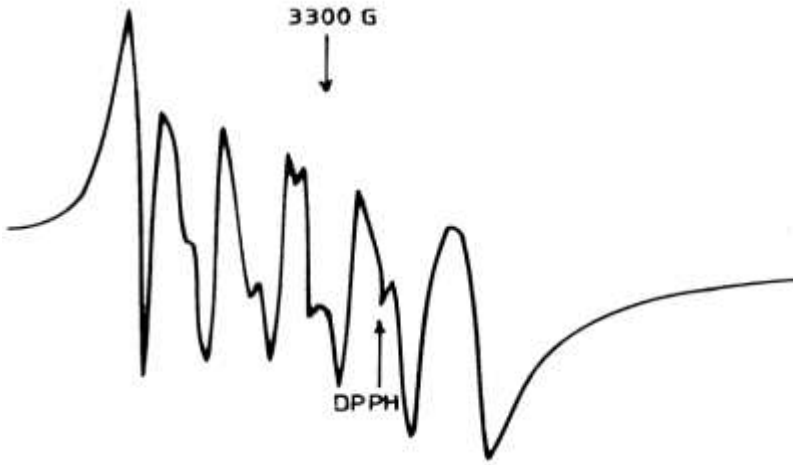

Fig. 11: ESR spectrum of $[Mn (PAPY)_2]Cl_2$ complex at 77 K

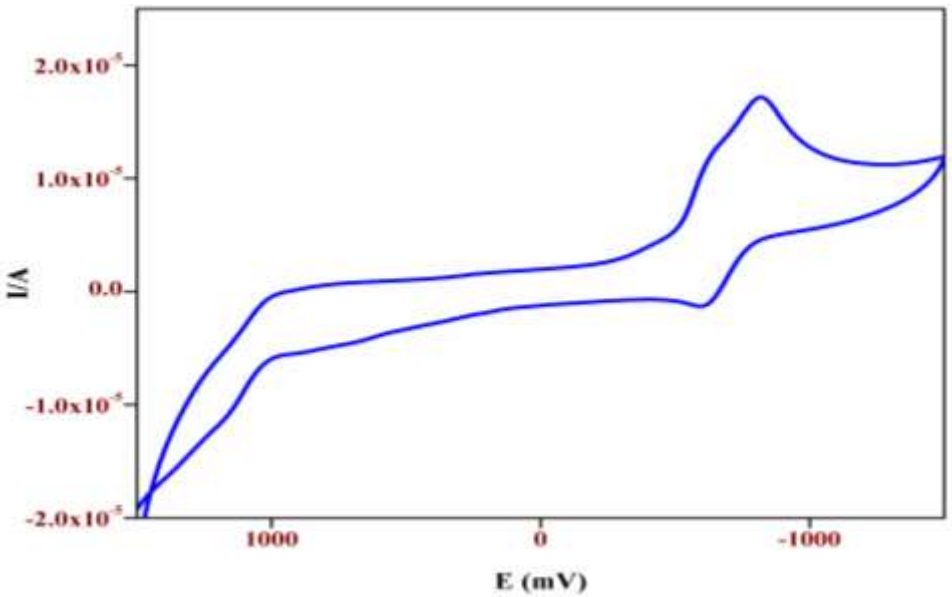

Fig. 12: Cyclic Voltammogram of $[Cu (PAPY)_2]Cl_2$ complex

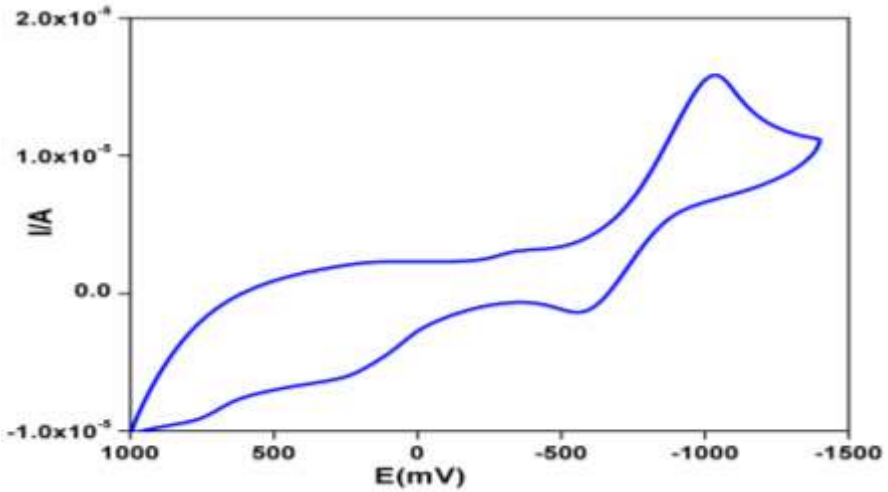

Fig. 13: Cyclic Voltammogram of [Mn (PAPY)$_2$]Cl$_2$ complex

Table 4
Electrochemical data of Pyrene based complexes (mV)

Compounds	Epc(mV)	Epa(mV)	ΔEp(mV)	Ipc/Ipa
(PAPY)$_2$Cu	982	595	387	0.56
(PAPY)$_2$Mn	863	528	335	0.36
(PAPY)Ni	1026	488	598	0.41

DNA binding mode and affinity of [Cu (PAPY)$_2$] and [Ni (PAPY)$_2$]: Electronic absorption spectroscopy is an effective method to examine the binding mode of DNA with metal complex. If the binding mode is intercalation, the π* orbital of the intercalated ligand can couple with the π orbital of the base pair, thus decreasing π-π* transition energy and resulting in the bathochromism. On the other hand, the coupling π orbital is partially filled by electrons, thus decreasing the transition probabilities and concomitantly resulting in hypochromism.

The binding affinity of the complexes of Cu (PAPY)$_2$ and Ni (PAPY)$_2$ with CT-DNA. DNA sample was added sequentially to Cu (II) complexes. The absorbance spectra were recorded after each addition and the changes in the spectral profiles during titration are shown in fig. 14 and fig. 15 The absorbance in the ligand absorption region as well as the MLCT bond decreased with increase in concentration of DNA.

In order to understand the DNA binding affinities of the two complexes quantitatively, the intrinsic DNA binding constant K_b was obtained according to equation 1, where [DNA] is the concentration of DNA band at a given DNA concentration; ε_f and ε_b are the molar absorption coefficient of the free Cu (II) complexes and the molar absorption coefficient of the Cu (II) complexes is fully bounded form respectively. ε_a is the molar absorption coefficient A_{abs}/ [M] of the MLCT absorption band at a given DNA concentration. K_b is the equilibrium binding constant in M^{-1}, C_t is the total Cu (II) complexes concentration and S is the binding site size

$$\frac{(\varepsilon_a - \varepsilon_f)}{(\varepsilon_b - \varepsilon_f)} = \frac{\left[b - \left(b^2 - 2K_b^2 C_t \frac{[DNA]^{1/2}}{S}\right)\right]}{2k_b C_1} \quad (1)$$

$$B = 1 + K_b C_t + K_b \frac{[DAN]_t}{2s} \quad (2)$$

The electronic spectrum of ligand has a strong band at 221nm, a medium band 323nm. They exhibit hypochromism of about 20 and 30% and red shift of about 3 and 1nm on complexation. In the spectra of the Cu (II) complex, the intense absorption bands with maxima at 202, 291 and 351nm are observed which are different from that of the ligand. In the presence of CT-DNA, the absorption bands of Cu (II) complex at 291, 351nm exhibit hypochromism of about 58 and 51%. The red shift is of about 12 and 6nm respectively.

However, the band at 202nm only exhibits hypochromism 21% and no evidence of red shift. It is noteworthy that the hypochromicity of the complex is greater than that of the parent ligand[10]. The intrinsic binding constants K_b of complexes [Cu (PAPY)$_2$] and [Ni (PAPY)$_2$] were 2.8×10^{-4} M^{-1} and $4.9 \times 10^{-4} M^{-1}$ respectively from the decay of the absorbance. The binding constant K_b of [Cu (PAPY)$_2$] complex is larger than the [Ni (PAPY)$_2$] complex.

It is indicated that [Cu (PAPY)$_2$] complex is bound to the DNA more tightly than the [Ni (PAPY)$_2$] complex[5]. This is due to the reason that in [Ni (PAPY)$_2$] complex, the presence of larger steric hindrance will reduce the interaction of the complexes with DNA.

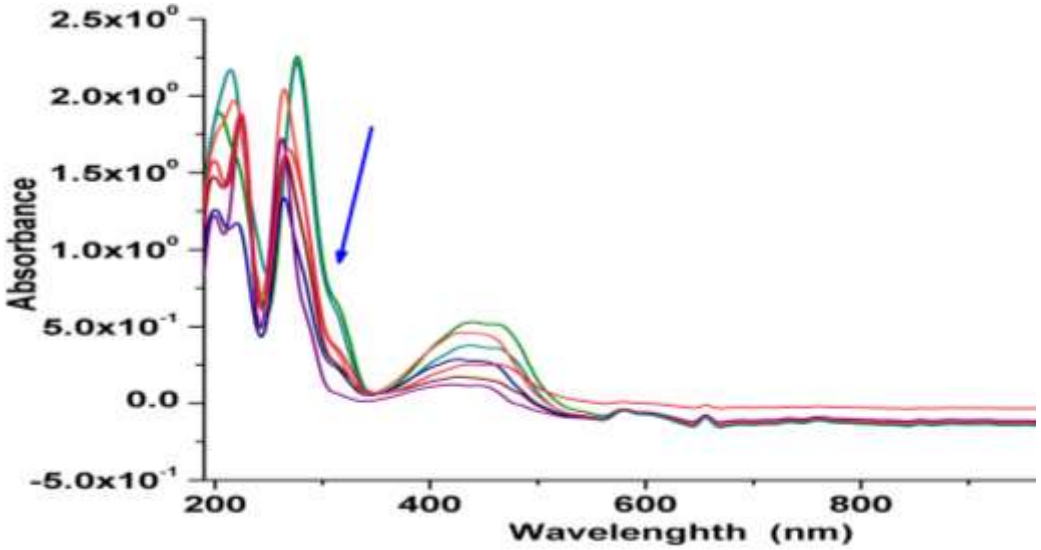

Fig. 14: UV-Vis spectrum of $[Cu (PAPY)_2]^{2+}$ complex showing absorption of spectral traces with increasing [DNA]

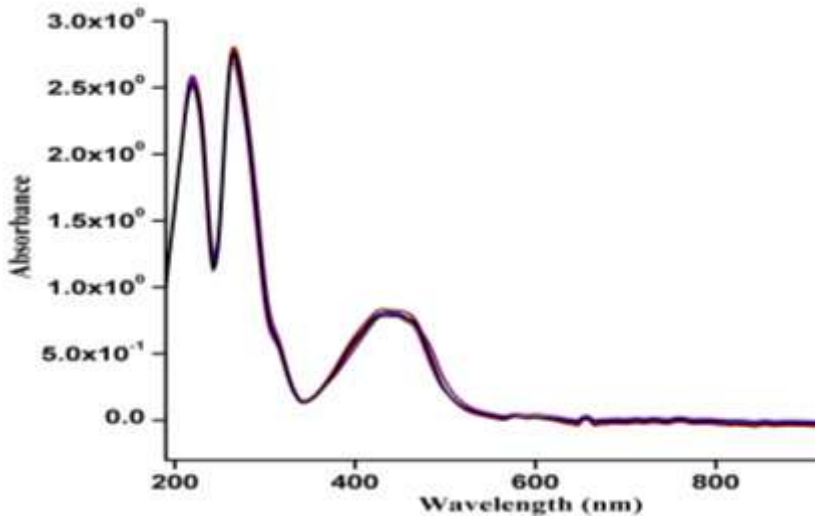

Fig. 15: UV-Vis spectrum of $[Ni (PAPY)_2]^{2+}$ complex showing absorption of spectral traces with increasing [DNA]

DNA Cleavage Studies: There has been considerable interest in DNA endo nucleolytic cleavage reactions that are activated by metal ions[14]. Coordination metal complexes have been used in majority of these cleavage studies.

Hydrolytic cleavage: The ability of complexes of Cu (II), Mn (II), Co (II), Ni (II) and Zn (II) to perform pUC18 DNA cleavage has been studied by agarose gel electrophoresis. When circular plasmid DNA is studied by electrophoresis, the fastest migration will be observed for the super coiled form (Form I). If one strand is cleaved, the super coils will relax to produce a slower-moving nicked circular form (Form II). If both strands are cleaved, a linear form (Form III) will be generated that migrates in between. Interestingly, the Ni (II) complexes show significant hydrolytic cleavage of SC DNA (Fig.18) under dark in aerobic conditions.

The PAPY and PAPY complexes display greater DNA cleavage activity than their Cu (II) and PAPY analogues. Although the DNA cleavage reaction through the complexes Cu (II), Mn (II), Co (II),Ni (II) and Zn (II) does not require additional external agents, we carefully investigated the possibility that diffusible HO° radical, singlet $^1O_2$ or superoxide anion radical $O_{2^{\cdot-}}$ were involved in this reaction. As shown in fig. 16, for Cu (II) complex, with an increase in time, the intensity of the both circular SC DNA (Form I) and nicked form (II) bands does not undergo any observable change (lane 2–7) as it is not a time dependent one.

Oxidative cleavage: As shown in fig. 17, the cleavage efficiency increases in the presence of H_2O_2 (lane 2-5) and singlet $^1O_2$ inhibitors. The same result was obtained in hydrolytic cleavage as well. But in oxidative process, the intensity of the nicked band increases compared to hydrolytic process. Even in presence of excess of H_2O_2 concentrations, the complex could cleave super coiled form (Form I) into slower-moving open circular form (Form II) only and complete conversion into form II and form III was not possible. The cleavage mechanism might involve hydroxyl radical oxidative mechanism. It is evident from the fig. 18 that both the complexes and H_2O_2 are required to cleave plasmid DNA.

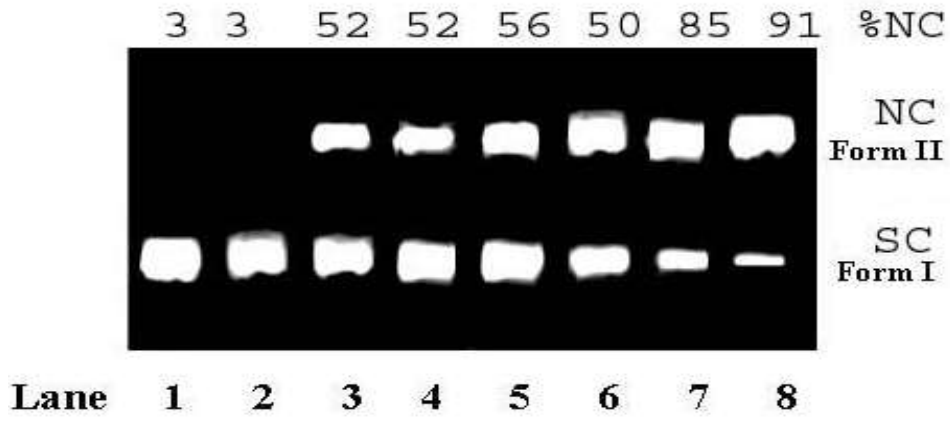

Lane 1.DNA Control, **Lane. 2.** DNA+DMSO, **Lane.3.** DNA+ PAPY.
Lane.4. DNA+ PAPY + DMSO, **Lane.5**. DNA + $[(PAPY)_2Cu]$,
Lane. 6.DNA+ $[(PAPY)_2Cu]$+ascorbic acid,
Lane. 7.DNA + $[(PAPY)_2Zn]$ +DMSO ,
Lane. 8. DNA+ $[(PAPY)_2Zn]$]+ascorbic acid
Ascorbic acid Complexes concentration was 35µM.
Forms I and II are super coiled and nicked circular, respectively

Fig. 16: Gel electrophoresis diagram showing the Cleavage of PUC 19 DNA

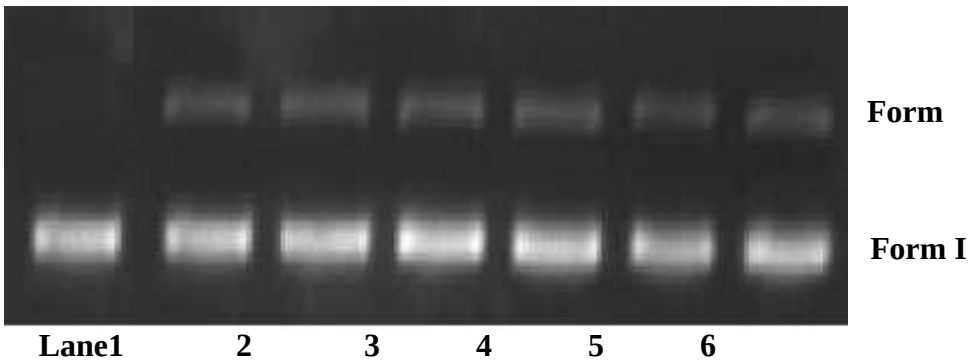

Lane 1: DNA, **Lane 2:** DNA + complex Zn (II) (100 µM) + 30 min,
Lane 3: Lane 2+ 60 min, **Lane 4:** Lane 2+ 90 min, **Lane 5:** Lane 2+ 120 min,
Lane 6: Lane 2 + 150 min, **Lane 7:** Lane 2 + 180 min

Fig. 17: Agarose gel electrophoresis diagram showing the cleavage of SCpUC18 DNA (500) mg by complex Cu (II) by various incubation time in Tris-Hcl buffer pH=7.1

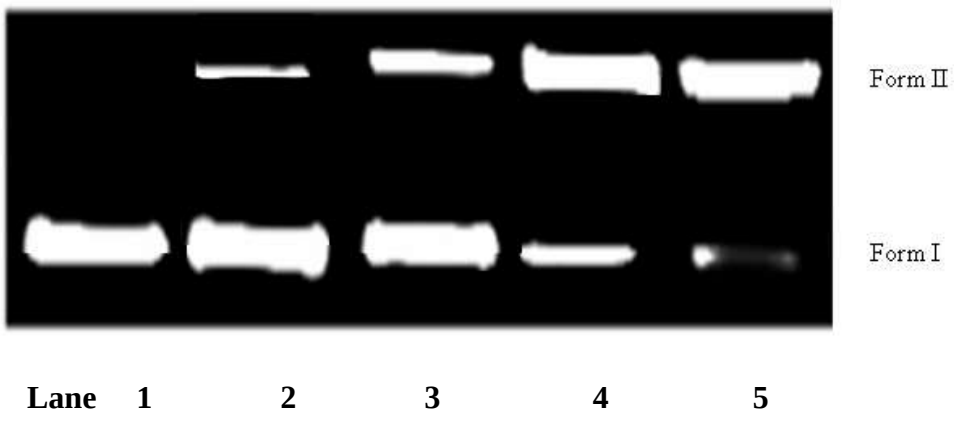

Lane 1: DNA, **Lane 2:** DNA + complex Ni (30 µM) +100 µM, **Lane 3**: DNA + complex Co (30µM) +100 µM H_2O_2**,**
Lane 4: DNA + complex Cu (30 µM) +100 µM H_2O_2, **Lane 5:** DNA + complex Zn (30 µM) +100 µM H_2O_2

Fig. 18: Agarose gel electrophoresis diagram showing the cleavage of SC pUC18 DNA (500 ng) by complexes Cu (II), Mn (II), Co (II), Ni (II) and Zn (II) in Tris-HCl buffer pH=7.1

Conclusion

A series of Mn (II), Co (II), Ni (II), Cu (II) and Zn (II) complexes has been synthesized with Schiff base ligand Synthesis of 1,5-dimethyl-2-phenyl-4-((pyren-1-ylmethylene)amino)-1H-pyrazol-3(2H)-one(1)(PAPY) is derived from 1-Pyrene carbox aldehyde and 4-aminoantipyrine.The structure of ligand and Mn (II), Co (II), Ni (II), Cu (II) and Zn (II) has been proposed through the analytical, spectral studies. DNA binding constants K_b of complexes [Cu $(PAPY)_2$] and [Ni $(PAPY)_2$] were 2.8 x $10^{-4}M^{-1}$ and 4.9 x $10^{-4}M^{-1}$ respectively from the decay of the absorbance.

The binding constant Kb of [Cu $(PAPY)_2$] complex is larger than the [Ni $(PAPY)_2$] complex. It is indicated that [Cu $(PAPY)_2$] complex is bound to the DNA more tightly than the [Ni $(PAPY)_2$] complex. This is due to the reason that in [Ni $(PAPY)_2$] complex, the larger steric hindrance will reduce the interaction of the complexes with DNA. In conclusion, the increased cleavage reaction in presence of H_2O_2 most probably occurs through a hydrolytic mechanism and the involvement of oxidation inhibitors.

References

1. Ahmad Shiekh R., Rahman I.A., Malik M.A., Luddin N., Malik Masudi S. and Thabaiti S.A., Transition Metal Complexes with Mixed Nitrogen-Sulphur (NS) Donor Macrocyclic Schiff Base Ligand: Synthesis, Spectral, Electrochemical and Antimicrobial Studies, *Int. J. Electrochem. Sci.*, **8**, 6972–6987 **(2013)**

2. Bagihalli G.B. and Patil S.A., Synthesis, Physico-Chemical investigations of Co(II), Ni (II) and Cu (II) complexes and there in vitro microbial, cytotoxic, DNA cleavage studies, *J. Enz. Inhi. Medi. Chem.*, **25**, 3430-439 **(2010)**

3. Christiane Marti and Erick Carreira M., Construction of Spiro [pyrrolidine -3,3′ -oxindoles] − Recent Applications to the Synthesis of Oxindole Alkaloids, *Eur. J. Org. Chem*., **12**, 2209-2219 **(2003)**

4. Clarke M.J., Ruthenium metallo pharmaceuticals, *Coord. Chem. Re.*, **236**, 209-233 **(2003)**

5. Eftnik R. and Ghiron C.A., Fluorescence quenching studies with proteins, *Anal.Biochem.*, **44**, 199-227 **(1981)**

6. Frieden E., Osaki S. and Kobayashi H., Mechanisms of oxidation with oxygen, *J. Gen. Physiol.*, **49(1 Suppl.)**, 213-252 **(1965)**

7. Granvoskii A.D., Uraev A.I. and Minkin V.I., Coord. Metal complexes from aryl and hetarylazocompounds, *Arkivoc*, **iii,** 29-41 **(2004**)

8. Irvin Noel Booysen, Sanam Maikoo, Matthew Piers Akerman and Bheki Xulu, Novel ruthenium (II) and (III) compounds with multidentate Schiff base chelates bearing biologically significant moieties, *Polyhedron.*, **79**, 250-257 **(2014)**

9. John Wilding P.H., The role of the kidneys in glucose homeostasis in type 2 diabetes: Clinical implications and therapeutic significance through sodium glucose co-transporter 2 inhibitors, *Metabolism*, **63(10),** 1228-1237 **(2014)**

10. Lacowicz J.R., Principles of Fluorescence Spectroscopy, third ed., Springer, New York **(2006)**

11. Laird P.W., The power and the promise of DNA methylation markers, *Nat. Rev. Cancer*, **3,** 253–266 **(2003)**

12. Macias B., Garcia I., Villa M.V., Borra S.J., Gonzalez A., lvarez M. and Casti~neiras A., Oxidative DNA damage of mixed copper (II) complexes with sulfonamides and 1, 10-phenanthroline: Crystal structure of [Cu(N-quinolin-8-yl-p-toluenesulfonamidate)2(1,10-phenanthroline)], *J. Inorg. Biochem.*, **96(2-3),** 367-374 **(2003)**

13. Mamdouh Masoud S. et al, Spectroscopic studies on some azo compounds and their cobalt, copper and nickel complexes, *Spect. Chim. Acta* (A), **60**, 2807 **(2004)**

14. Shahabadi N., Kashanian S. and Darabi F., Regioselective synthesis and molecular modelling study of vasorelaxant active 7, 9-dioxa-1, 2-diaza-spiro [4.5] dec-2-ene-6, 10-diones, *Euro. J. Med. Chem.*, **45(9)**, 4239-4245 **(2010)**

15. Sugiura Y., Hirayama Y., Tanaka H. and Ishizu K., Copper (II) complex of sulfur-containing peptides, Characterization and similarity of electron spin resonance spectrum to the chromophore in blue copper proteins, *J. Am. Chem. Soc*., **97**, 5577-5581 **(1975)**

16. Tu B., Li R.R., Liu Z.J., Chen Z.F., Ouyang Y. and Hu Y.J., Structure-activity relationship study between baicalein and wogonin by spectrometry, molecular docking and microcalorimetry, *Food Chem*., **208**,192-198 **(2016)**

17. Tudor Rosu, Maria Negoiu, Simona Pasculescu, Elena Pahontu, Donald Poirier and Aurelian Gulea, Metal-based biologically active agents: Synthesis, characterization, antibacterial and antileukemia activity evaluation of Cu(II), V(IV) and Ni(II) complexes with antipyrine-derived compounds, *Eur. J. Medi. Chem.*, **45**, 774-781 **(2010)**

18. Wilmot B., Fry R., Smeester L., Musser E.D., Mill J. and Nigg J.T., Methylomic analysis of salivary DNA in childhood ADHD identifies altered DNA methylation in VIPR2, *J. Child Psychol. Psyc*., **57**, 152-160 **(2016)**.

(Received 24th June 2020, accepted 30th August 2020)